Cerebral Cortex, March 2017;27:2195–2209

doi:10.1093/cercor/bhw071
Advance Access Publication Date: 21 March 2016
Original Article

ORIGINAL ARTICLE

Clonal Mapping of Astrocytes in the Olfactory Bulb and Rostral Migratory Stream

Jorge García-Marqués[1,2] and Laura López-Mascaraque[1]

[1]Instituto Cajal-CSIC, 37 28002 Madrid, Spain and [2]Current address: Janelia Research Campus, Howard Hughes Medical Institute, Ashburn, VA 20147, USA

Address correspondence to Laura López-Mascaraque. Email: mascaraque@cajal.csic.es

Abstract

Astrocytes are the most abundant glial population in the central nervous system, where they fulfill multiple essential tasks. Such diverse functions require a heterogeneous population of cells, yet it is still unclear how this cellular heterogeneity emerges during development. To clarify to what extent such diversity is determined by lineage, we have elaborated the first clonal map of astrocytes in the olfactory bulb and rostral migratory stream. Astrocyte clones are comprised of a limited number of cells, which arise from local progenitors and that are arranged following a radial pattern. Although astroglia exhibit a vast morphological diversity, this was layer-dependent rather than determined by lineage. Likewise, lineage did not strictly determine their position, although we found a striking relationship between the clones and olfactory glomeruli. A distinctive morphology and other clonal features, together with the occurrence of immature forms, reflect the singularity of these astroglial populations.

Key words: astroglia, clonal analysis, development, gliogenesis, star track

Introduction

Astrocytes are the most abundant glial population in the vertebrate brain and although originally described as a homogeneous cell population, the functional and morphological diversity of these cells is now well established (Matyash and Kettenmann 2009; García-Marqués et al. 2010; Zhang and Barres 2010; Oberheim et al. 2012). The existence of such a heterogeneous cell population upholds its role as a fundamental element in multiple brain functions. In particular, astrocytes are crucial for metabolic and structural support, vasomodulation, information processing, recovery from injury, synaptogenesis, and the establishment of the blood brain barrier, among others (reviewed in Wang and Bordey 2008).

Astroglial heterogeneity is associated with the multiple developmental origins of these cells. In the rodent central nervous system (CNS), astrocytes emerge from at least 2 different progenitors (reviewed in Levison and Goldman 1993). Radial glia can give rise to intermediate astroglial progenitors during embryogenesis and at early postnatal stages, which subsequently migrate from the ventricular/subventricular (VZ/SVZ) region. Once these progenitors reach their final destination, they proliferate to produce groups of sibling astrocytes by undergoing symmetric cell divisions (García-Marqués and López-Mascaraque 2012; Ge et al. 2012). This process leads to a certain level of clonal compartmentalization, with clones of different sizes occupying different areas. Subsequently, astrocytes may also arise through the direct transformation of radial glia whose cell bodies translocate in conjunction with the shortening of their radial process. Furthermore, as astroglial progenitors are distributed along the entire neural tube, these different spatial origins further contribute to the diversity of these cells (Hochstim et al. 2008; Chaboub and Deneen 2012).

Few studies have focused on the direct link between the identity of single progenitors and their astroglial progeny. In the cerebral cortex, clonal analysis demonstrated the existence of progenitors with different grades of pluripotency, producing cohorts of astrocyte clones of different sizes and at distinct locations (Price and Thurlow 1988; Walsh and Cepko 1988; McCarthy et al. 2001). However, the lack of a suitable method has limited these analyses to just a few brain regions. Indeed, classical clonal analyses based on embryonic retroviral injections fail to target

the glia in regions like the olfactory bulb (OB: Reid et al. 1999), as well as other glial populations.

Having recently developed Star Track, a technique suitable to track families of astrocytes (García-Marqués and López-Mascaraque 2012), we set out to examine the clonal fate of astrocytes generated in the OB and rostral migratory stream (RMS). This analysis revealed that the generation of astrocytes in the OB and RMS occurs as a well-organized radial process, with a few obvious limitations to their clonal organization. In the OB, astroglial clones occupy several layers depending on their size and there was a striking association between these clones and the olfactory glomeruli. Their unusual clonal features, the extreme diversity of morphologies, and the presence of immature glial forms highlight the singularity of these populations.

Materials and Methods

Animals

C57 mice bred at the Cajal Institute's animal facility were used in this study, and they were handled in compliance with current Spanish legislation (R.D. 1201/2005 and L. 32/2007) and European Union Council Guidelines (2010/63/EU) regarding the care and use of experimental animals. The day of detection of the vaginal plug and the day of birth were considered as E0 and P0, respectively. Early post-natal mice (up to P5) were anesthetized by hypothermia, whereas adult mice (from P30 onward) were anesthetized by intraperitoneal injection of Equithesin (3 mL/kg body weight).

Tissue Processing and Immunohistochemistry

After anesthesia, early postnatal and adult mice were perfused transcardially with 4% paraformaldehyde (PF) in 0.1 M phosphate buffer (PB, pH 7.2). The brain of each mouse was then post fixed in PF for 2 h at 4°C and coronal vibratome sections (100 μm for Star Track general analysis and 50 μm if used for immunohistochemistry) were obtained. Draq5 was used for nuclear counterstaining.

For immunohistochemistry, vibratome brain sections (50 μm) were transferred to phosphate buffer saline (PBS) containing 0.1% Triton X-100 (PBS-T) for 5 min and then blocked for 30 min in a solution of 2% bovine serum albumin (Sigma) diluted in 0.1% PBS-T. The sections were then incubated overnight with an anti-glial fibrillary acidic protein antibody (GFAP, 1:500: Dako) in the same blocking solution and on the next day, they were rinsed in 0.1% PBS-T and incubated for 90 min with a biotinylated anti-rabbit IgG secondary antibody (1:200: Vector Laboratories) in 0.1% PBS-T. After further rinsing, the sections were incubated for 2 h with Alexa 633 conjugated streptavidin (Molecular Probes, 1:2000) in a solution of 0.1% PBS-T. Finally, the sections were rinsed, mounted onto slides in PB/Glycerol (1:1), and sealed with nail polish.

In Utero Electroporations

Pregnant mice were anesthetized with isofluorane (Isova vet, Centauro), and their uterine horns were exposed through a midline incision in the skin and abdominal wall. The uterus was trans-illuminated with cold light and 2 μL of the Star Track plasmid mixture (2–5 μg/μL DNA in 0.1% fast green: García Marqués and López-Mascaraque 2012) was injected into the lateral ventricles of E14 embryos using a glass micropipette oriented in caudo-rostral direction. The embryos were then pat dried to avoid current dispersion across less resistive pathways. After injecting all the embryos, they were placed between the disks (3 mm diameter) of a tweezer-type electrode (previously moistened with saline) and 1 or 2 trains of 5 square pulses were applied (33 V; 50 ms followed by 950-ms intervals) using a noncommercial electroporator. Due to the difficulty of electroporating in the OB/RMS, the electrodes position was decisive. The disk center was placed optimally 0.5 mm anterior to the eye bud or slightly posterior for RMS electroporations. Embryos were held between both disks, applying enough pressure to maintain the maximal surface of both disks in direct contact with the tissue but not enough to damage the embryo. Afterward, the uterine horns were placed back into the abdominal cavity, filling this with warm physiological saline, and the abdominal muscle and skin were closed with absorbable polyglycolic acid (Surgicryl) and silk (5/0: Lorca-Marin) sutures, respectively. Finally, pregnant mice received a subcutaneous injection of the antibiotic enrofloxacine (5 mg/kg: Baytril, Bayer) and an intraperitoneal injection of the anti-inflammatory/analgesic meloxicam (300 μg/kg: Metacam, Boehringer Ingelheim).

Imaging Settings

Images were obtained on a Leica TCS-SP5 confocal microscope, acquiring 2 or 3 different channels simultaneously. The excitation and absorption conditions for each fluorophore were (in nm): mT-Sapphire (Ex 405, Ab 525–553), mCerulean (Ex 458, Ab 464–481), EGFP (Ex 488, Ab 496–526), YFP (Ex 514, Ab 520–543), mKusabira Orange (mKO: Ex 514, Ab 550–600), mCherry (Ex 561, Ab 601–612), and AlexaFluor 633/Draq5 (Ex 633, Ab 649–760). Each channel was assigned as the emission color, except for mT-Sapphire that was assigned as dark blue and Alexa Fluor 633/Draq5 assigned as gray. The maximum intensity projections for each channel were adjusted uniformly and overlapped using Adobe Photoshop CS5 software. OB 3D reconstruction was generated using the image software Fiji (Schindelin et al. 2012).

Data Analysis

Brain sections (100 μm) from 3 different animals electroporated at E14 (each from a different litter) were analyzed serially. Every cell was numbered and examined for the presence/absence of each fluorophore. This combination was considered as a 12-digit binary signature (0 = absence, 1 = presence: following the order of cytoplasmic mCerulean, mTSapphire, GFP, YFP, mKO, and mCherry, and then the same order for the nuclear markers). Once each labeled cell had been cataloged, the combinations repeated in more than 2 separate electroporations were discarded from the further analysis. Where only nuclear markers were detected, the cells were not considered as they impeded us from configuring the glial morphology. As such, we defined those cells sharing the same combination of fluorophores/signature as clones, as long as the pattern was not repeated in more than 2 separate electroporations.

To estimate the radial dispersion of clones, we used Fiji to measure the length of the line connecting each soma to the center of the subependymal zone (SEZ). The radial expansion was then defined as the difference between the minimal and the maximal dispersion of the cells. Similarly, dispersion in the rostrocaudal axis was estimated as the distance between the first and the last slice containing cells of that clone. Statistical analyses were performed in Prism (Graphpad) using Spearman's rank coefficient correlation and linear regression parameters.

Results

Star Track Enables a Clonal Analysis of Astrocytes to be Performed in the OB

In an attempt to reveal the relationships underlying the familiar arrangement of astrocytes in the OB, we employed Star Track on

E14 mouse embryos, a lineage-tracing method based on the electroporation of multiple plasmids driving the expression of up to 12 different fluorescent proteins in the cytoplasm or nucleus (Fig. 1A: García-Marqués and López-Mascaraque 2012). Following their transposon-mediated random integration, progenitor cells acquire a unique and inheritable mixture of these sequences, which allows their progeny to be identified as those cells sharing the same unambiguous markers/signature. After performing in utero electroporation of the Star Track plasmids at E14, small groups of cells exhibiting the same lineage-specific markers were evident as early as P0 (Fig. 1B,C, arrow). In the outer layers, these groups were arranged as small clusters of up to 10 cells, characterized by large branched processes emanating from their soma (Fig. 1B). This contrasted with the inner layers, where only single cells or pairs of cells were evident, and the cells resembled radial glia, with long processes running transversally towards the pial surface (Fig. 1C). Occasionally, these pairs consisted of 2 cells projecting their processes in opposite directions, which suggested a recent mitosis (Fig. 1C, arrowhead). By illustrating the first phases of astrocyte generation, we confirmed that Star Track efficiently targets astrocytes in the OB.

OB and RMS Astrocytes are Derived From Local Progenitors

To better understand which proliferative regions contribute to the generation of OB/RMS astrocytes, we analyzed serial sections from adult brains after the electroporation of the Star Track plasmids at E14 (Fig. 2). Electroporation of the olfactory ventricle proved to be challenging and most of our initial electroporations were restricted to the anterior part of the lateral ventricle (as shown in Fig. 2A,C). Such procedures labeled glial-cells in all the cortical layers, although there was no glial labeling in either the ipsilateral or contralateral OB or RMS ($n \geq 15$, independent electroporations from different animals or hemispheres; García-Marqués et al. 2014). Similarly, we also performed electroporations that labeled glia in the cortex, RMS and OB ($n = 5$; Fig. 2A–E), these labeled glia appearing only on the electroporated side (Fig. 2B,D). In contrast, on the non-electroporated side only small cells that were very weakly labeled could be detected, these cells predominantly scattered across the granular cell layer (GCL) of the OB (Fig. 2B,E). This labeling corresponded to the residual fluorescence found in neuroblasts arising from GFAP-positive progenitors (García Marqués and López-Mascaraque 2012). Along with the labeling found in SVZ/VZ that surrounded the lateral ventricles, it appeared that our electroporation had reached more posterior areas. In addition, we also found glial labeling restricted to the OB, which reflected electroporation that targeted the most anterior tip of the olfactory ventricle ($n = 4$: Fig. 2F–K). In these cases the most posterior labeling was found in slices that included the OB and anterior olfactory nucleus (Fig. 2F,J–K), and multiple glial clones were evident in the electroporated side (Fig. 2G,H). However, in contrast to those electroporations that reached the lateral ventricle (Fig. 2B,E), there was virtually no residual labeling in the nonelectroporated side in these brains (Fig. 2G–I). In conjunction, with the restricted labeling on the electroporated side, the independent patterns witnessed provided evidence of the local origin of the OB/RMS glial population.

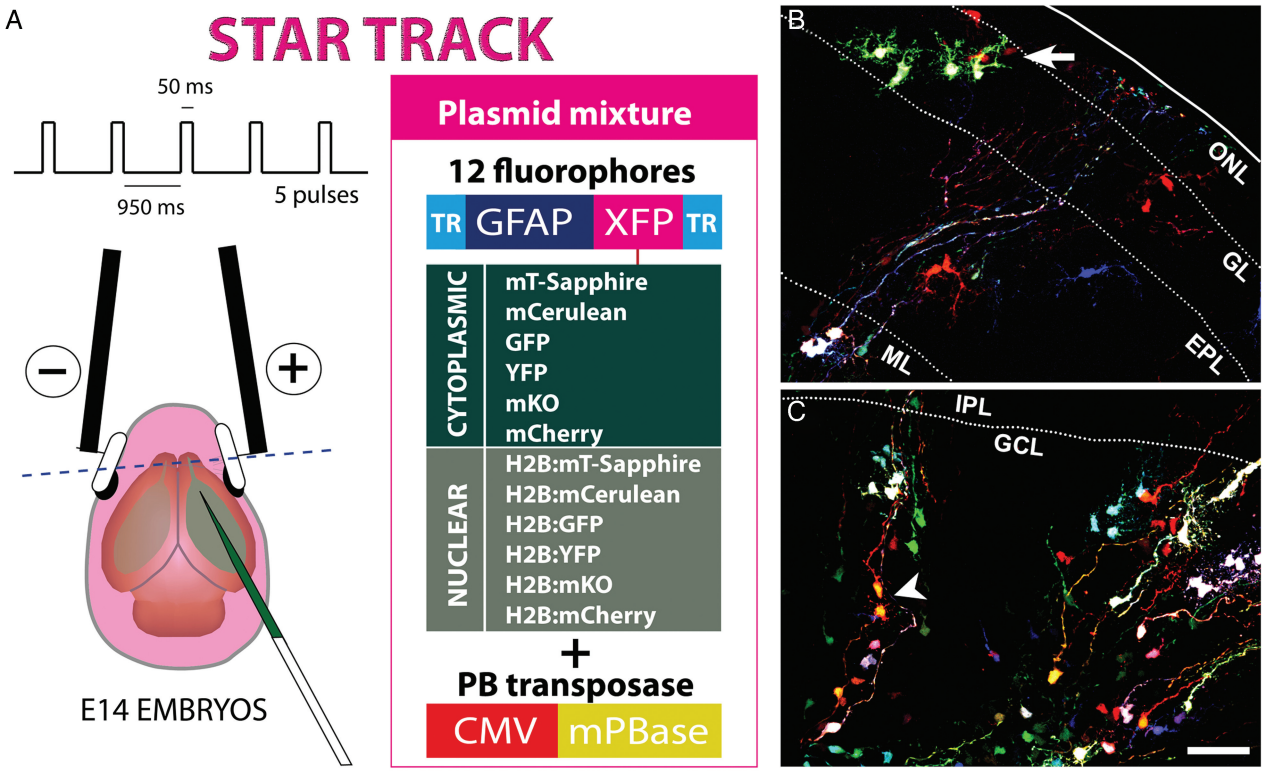

Figure 1. Star Track enables a clonal analysis of OB astrocytes to be performed. (*A*) Star Track constructs and electroporation protocol. TR: PiggyBac terminal repeats. (*B*) Outer OB layers in a P0 mouse electroporated at E14. Groups of cells sharing the same fluorescent signature (arrow) (*C*). Inner OB layers in a P0 mouse electroporated at E14. Note the appearance of cell pairs with the same fluorescent signature that project their radial processes in opposite directions (arrowhead). Scale bars = 50 μm in *B* and *C* (shown in *C*).

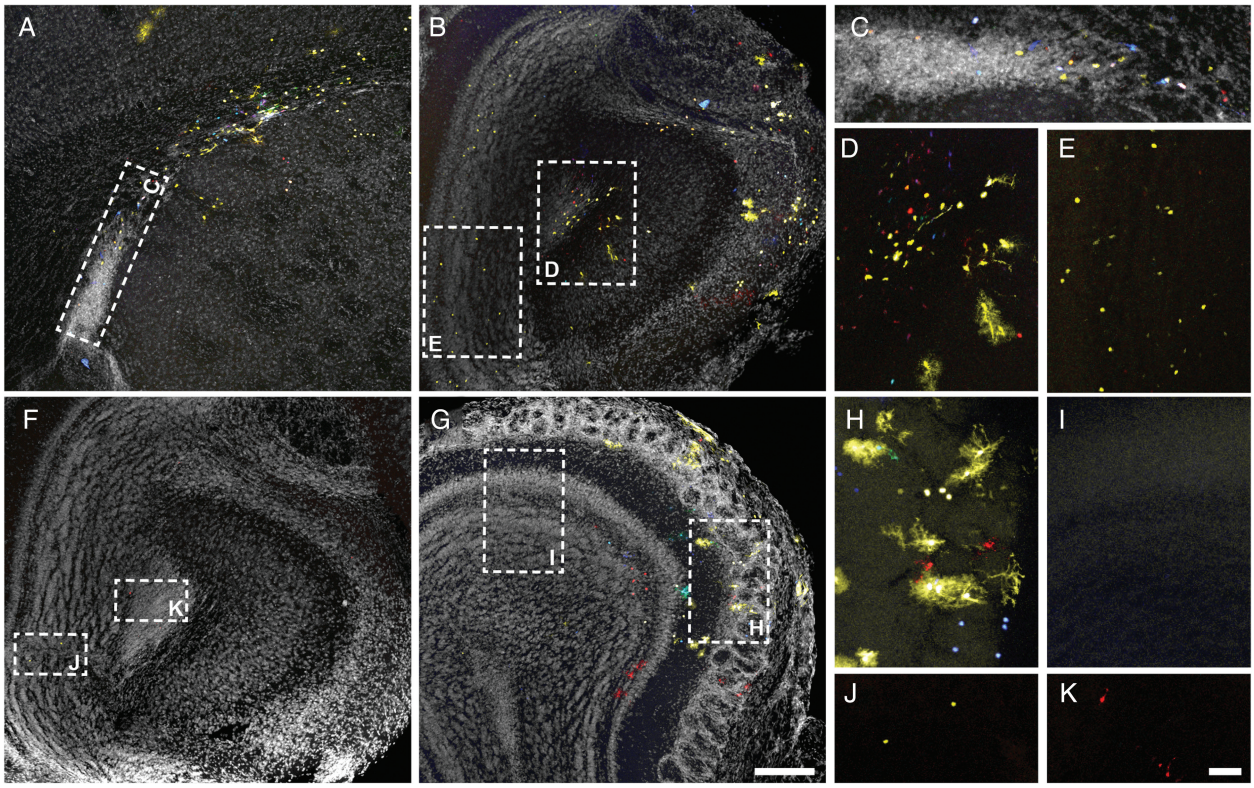

Figure 2. Local generation of OB and RMS astroglia. Adult brain sections after Star Track electroporation at E14. (*A–E*) Extensive electroporation targeting the lateral (*A*,*C*) and olfactory ventricle (*B*,*D–E*). (*C–E*) Higher magnification of insets in A (*C*) and B (*D–E*). (*F–K*) Electroporation restricted to the rostral olfactory ventricle. (*F*) Most caudal section with labeled cells. (*H–K*) Higher magnification of insets in F (*J–K*) and G (*H*,*I*). Residual labeling in the nonelectroporated side is exclusively found in electroporations targeting the SVZ in the lateral ventricles (compare *E* and *I*). Nuclear counterstaining is shown in gray. Scale bars = 200 μm in *A*,*B*, *F*,*G* (shown in *G*); 50 μm in *C–E*, *H–K* (shown in *K*).

Astrocytes Disperse Along Precise Radial Pathways: a Study of Their Morphology and Clonal Organization in the OB

In the OB, Star Track-labeled cells dispersed across all layers in a strict fan-shape originating in the SEZ (Fig. 3*A–F*). As these electroporations only targeted one side of the ventricle, a restricted pathway of radial migration was confirmed and only a few labeled cells were located in the contralateral side (Fig. 3*A*,*B*, arrowheads). Our analysis also revealed an extraordinary morphological heterogeneity, with few cells adopting a typical protoplasmic morphology. However, we did not find an obvious relationship between morphology and clonal status, rather astrocyte morphology appeared to be more layer-dependent. Remarkably, the cells were organized along a morphological gradient whereby the inner layers contained cells with fewer processes than those in the outer layers, the latter populated by astrocytes with multiple and extensively branched processes (Fig. 3*A–F*; Fig. 6). In the olfactory nerve layer (ONL) and pial surface, astrocytes were predominantly organized as cytoplasmic sheets and they occasionally sent thick processes into the glomerular layer (GL; Fig. 3*G–O*; Fig. 6*A*,*B*). These astrocytes were distributed in small clonal clusters of cells that shared the same color signature (Fig. 3*G–I*), similar to the pial clones described in the cerebral cortex (García Marqués and López-Mascaraque 2012). In both the ONL and GL, the fluorescent labeling of astrocytes was particularly intense, perhaps reflecting the stronger activity of the GFAP promoter (Fig. 3*G–O*). A clear morphological barrier separated the GL and the external plexiform layer (EPL; Fig. 3*J–O*) and whereas GL astrocytes displayed thicker processes (Fig. 3*J–O*; Fig. 6*C*,*D*), EPL astrocytes had a markedly protoplasmic morphology, characterized by a spherical projection of fine branched processes (Fig. 3*J–O*; Fig 6*E*,*F*). The clonal organization of these layers was reflected by the multiple small clones that coexisted in close proximity. In the EPL, such organization was random, with no obvious relationship to OB anatomy (Fig. 3*J–O*; Fig 6*E*,*F*). However, the clonal clusters in the GL were organized according to the glomerular anatomy. Indeed, most clusters populated one or few adjacent glomeruli (Fig. 4; Supplementary Movie 1), with their somata situated either at the walls (Fig. 4*A–H*; Fig. 6*C*) or within the glomerular neuropil (Fig. 4*I–L*; Fig. 6*D*).

Due to the higher density and smaller cell size, we studied the clonal organization in the deeper layers of the OB using serial sections with scarce labeling (Fig. 5*A–L*). Cell morphology in the mitral layer (ML), internal plexiform layer (IPL) or outer GCL (oGCL) was relatively similar, and despite their extensive catalog of shapes, astrocytes in these layers showed less exuberant processes while retaining a certain protoplasmic aspect (Fig. 5*G–K*; Fig. 6*F–J*). This changed in the deeper GCL (dGCL) and SEZ, where the cells exhibited a rudimentary morphology with few and poorly branched processes (Fig. 5*L*; Fig. 6*K–M*). In terms of the clonal arrangement, astrocytes in the ML, IPL, and oGCL formed clonal clusters the size of which was not substantially different to those in the external layers. However, these clusters were considerably smaller in the dGCL and SEZ, where few cells sharing the same signature constituted most of the clonal groups (Fig. 5*L*). Like the external layers, we did not observe absolute

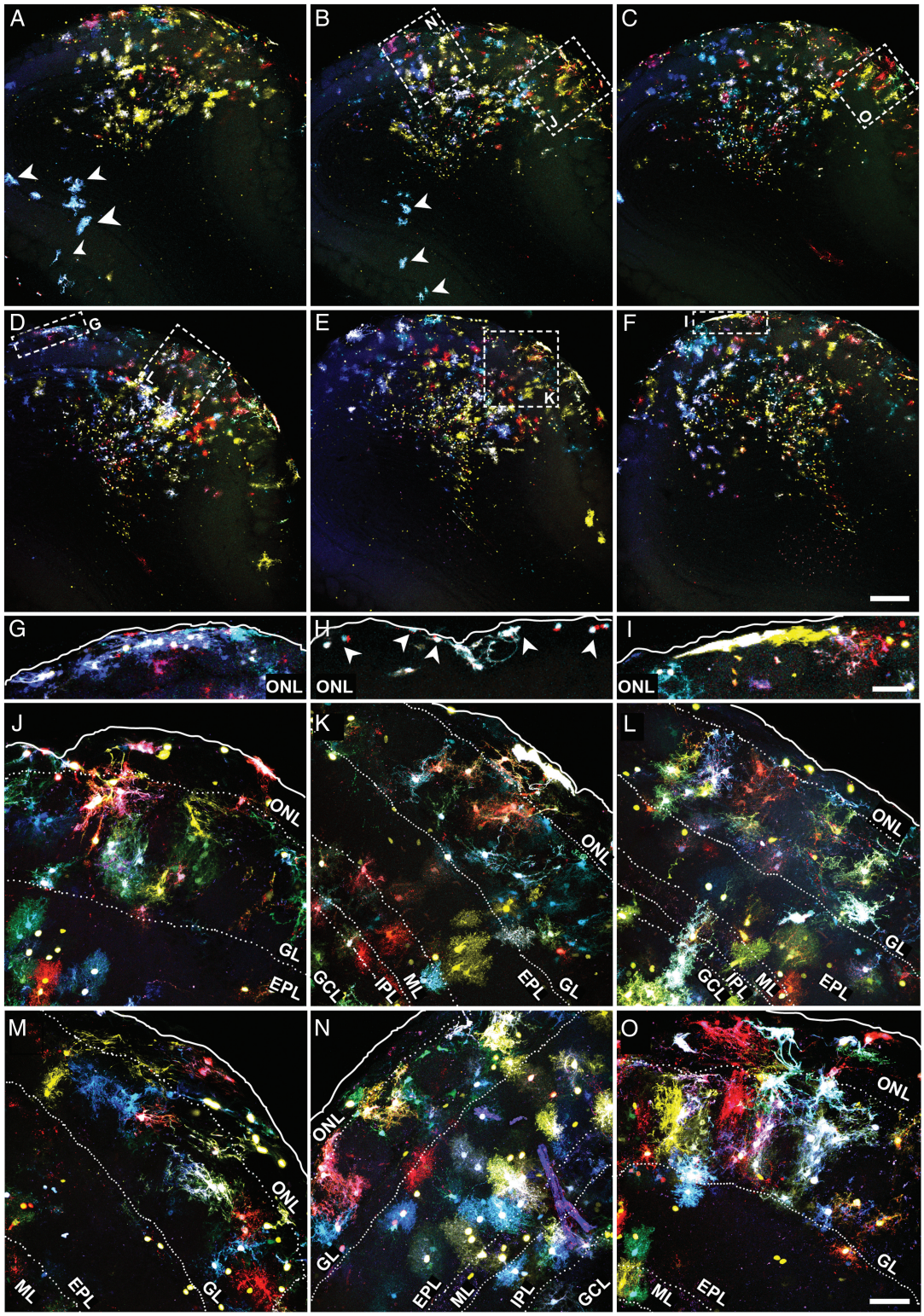

Figure 3. Astroglial clonal organization in the adult OB (external layers). Adult brain sections after Star Track electroporation at E14. (*A–F*) Low magnification serial sections (rostral to caudal from left to right, top to bottom). (*G–I*) Amplified view of the pial clones in the ONL/pia of the above (*G* and *I* correspond to *D* and *F*, respectively) or analogous sections. (*J–O*) Magnified view of outer OB layers showing astrocyte clones labeled with Star Track from the above (*J–N*, *K,O,L* corresponding to *B,E*, *C*, and *D*, respectively) or analogous sections. Scale bars = 200 μm in *A–F* (shown in *F*); 50 μm in *G–I* (shown in in *I*), and *J–O* (shown in *O*).

layer restriction of clonal groups in the deeper layers, and only small clonal clusters appeared to be restricted to a single layer. Nevertheless, many of the clusters that settled between 2 layers adapted their processes to this anatomy, especially those between the GCL and IPL (Fig. 5*G*,*H*; Fig. 6*G*). In summary, OB clones were distributed radially over one or several layers and these clones contained cells with varied morphologies, although they never spanned its entire radial extension.

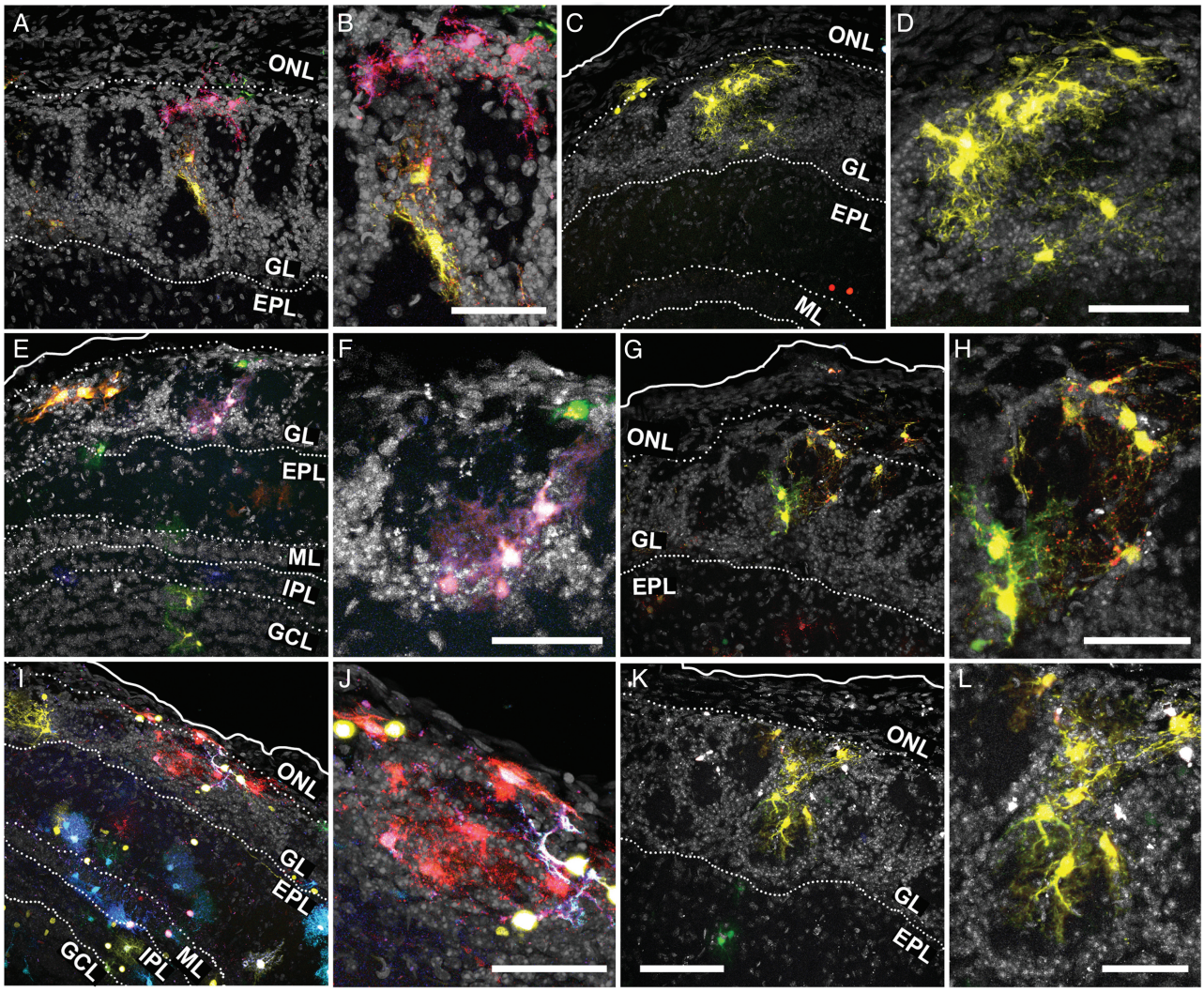

Figure 4. Clonal astrocyte arrangement in the adult olfactory glomeruli. Adult sections from brains electroporated at E14 with Star Track. (*A–H*). Astrocyte clones arranging their somata in the walls of a single or few glomeruli, shown at low (*A,C,E,G*) or high magnification (*B,D,F,H*). (*I–L*) Astrocyte clones with most of their somata located in the neuropil of a single glomerulus, shown in low (*I,K*) or high magnification (*J,L*). Nuclear counterstaining in gray. Scale bars = 100 μm in *A,C,E,G,I,K* (shown in *K*); 50 μm in *B,D,F,H,J,L*.

Quantitative Analysis of Astrocyte Families in the Adult OB

An unambiguous description of clones required to locate all the astrocytes comprising each family. To this end, a reference was assigned to every labeled cell within the OB and its fluorescent label was encoded as a 12-bit string or signature that reflected the presence/absence of each fluorophore (Table 1; Supplementary Fig. 1–4). After discarding those cells without any cytoplasmic labeling, we selected 42 clones with a singular mark (Fig. 7A; Supplementary Fig. 5), defined as those detected in less than 2 separate electroporations. In this way we excluded strings usually composed of a limited number of fluorophores, which tended to appear with higher frequency. This makes it extremely unlikely to find the same string as 2 independent events (García Marqués and López-Mascaraque 2012). Our analysis in the adult OB identified clones that ranged in size from 1 to 65 cells, with an average of 6.95 cells. We also found that 10 out of 42 clones represented single-cell families. In terms of their distribution, there was some relationship between the clonal size and the number of layers occupied. Except for the clones distributed in the GCL, the largest layer in terms of volume (Table 1, e.g., clone #5 and 6), most of the clones distributed over a single layer were comprised of one cell. This was the case of clones #26, #35 and #39, which exclusively populated the GL, and only clone #13 contradicted this rule, containing 5 cells restricted to the MT layer. Moreover, most of the multi-cell clones colonized adjacent layers, exhibiting continuity in terms of their dispersion. Interestingly, only clone #40 contained cells in the SEZ. In the rostrocaudal dimension, clones also appeared as clusters, with most of the cells distributed across contiguous slices (Fig. 7A and Table 1).

To clarify how the volumetric expansion of clones was related to the clonal cell count, we performed a correlation analysis between the rostrocaudal and radial dispersion in terms of the number of cells in each clone (Fig. 7B,C). As expected, the cell count was strongly and positively correlated to both the radial (Fig. 7B; Spearman correlation, $P < 0.0001$; $\rho = 0.72$) and rostrocaudal dispersion (Fig. 7C; Spearman correlation, $P < 0.0001$; $\rho = 0.77$). However, a linear regression model could not explain such a correlation, as the variance for both dispersions increased with the clonal cell count ($R^2 = 0.2$ for radial and $R^2 = 0.17$ for rostrocaudal dispersion).

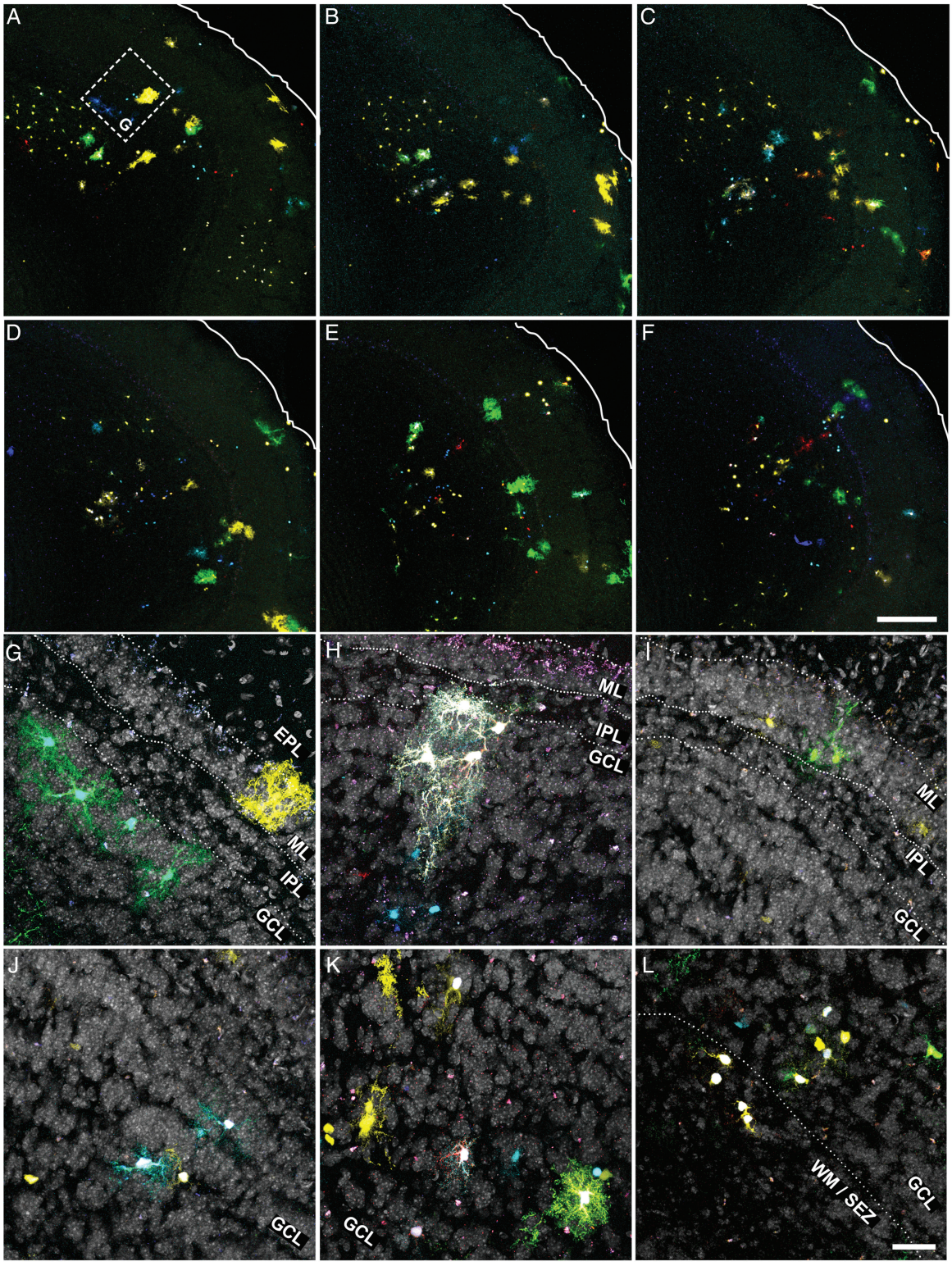

Figure 5. Astroglial clonal organization in the adult OB (internal layers). (*A–F*) Low magnification of adult OB serial sections after Star Track electroporation at E14 (rostral to caudal from left to right, top to bottom). (*G–I*) High magnification of astrocyte clones in the ML to oGCL layers (*G–I*) and dGCL/SEZ (*J–L*) from the above (*G* corresponding to A) or analogous sections. Nuclear counterstaining shown in gray. Scale bars = 200 μm in *A–F* (shown in *F*); 50 μm in *G–L* (shown in *L*).

Reminiscences of Immature Glia in the OB

In the course of our clonal analysis in the adult OB, we distinguished the presence of long processes similar to those of radial glia. To determine whether immature glia might be present in the adult OB, we took advantage of the single-cell resolution achieved by Star Track in low-density labeled sections. In these sections we could identify cells projecting radial processes in different directions, mainly transversal to the OB surface (Fig. 8A–C).

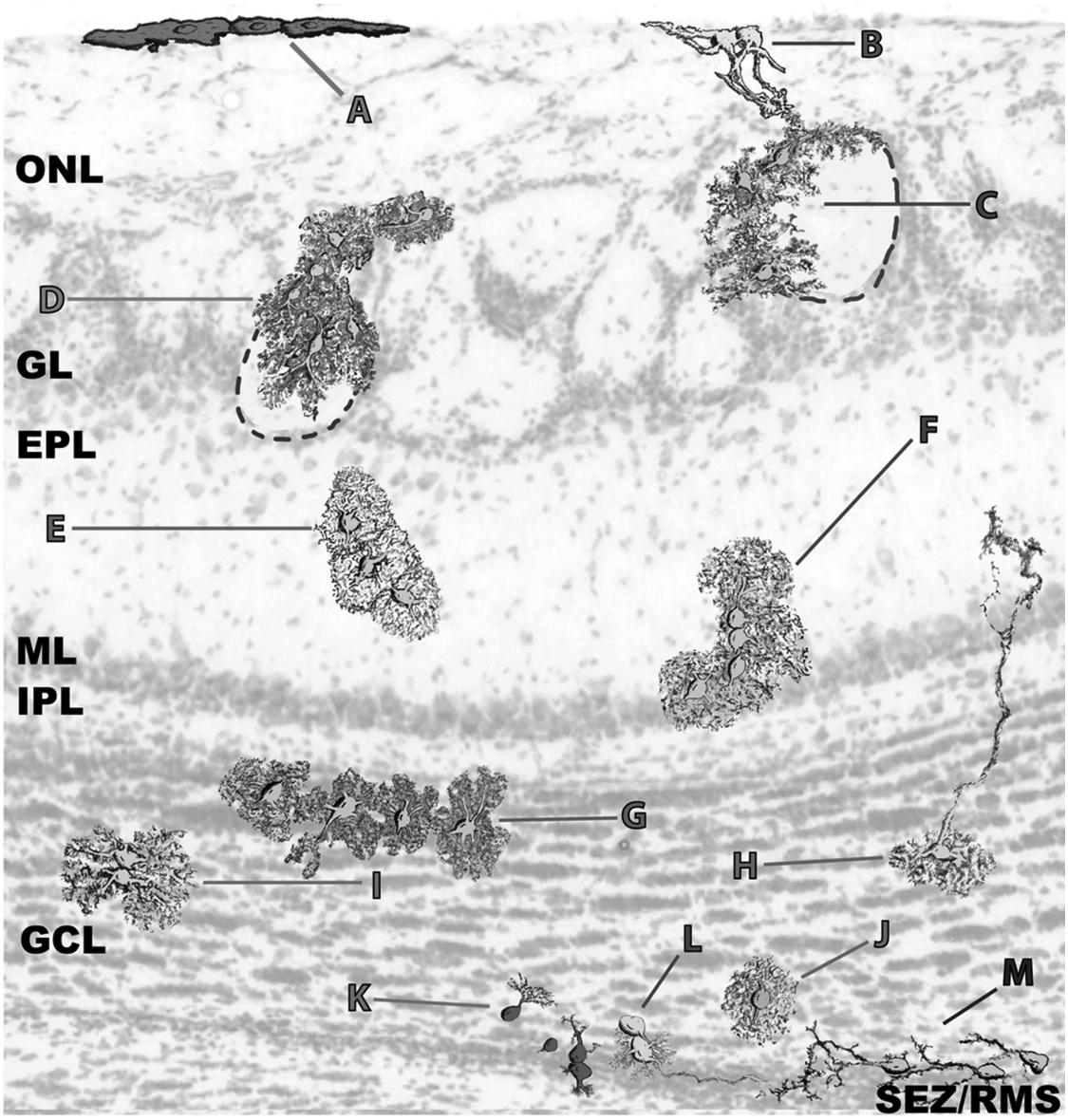

Figure 6. OB and RMS astroglia exhibit a vast morphological diversity. (*A*) Pial clones exhibiting a sheet-like morphology. (*B*) ONL astroglia projecting thick processes into the GL. (*C*) Clones with their somata distributed over the interglomerular walls. (*D*) Clones with their somata gaining access to the glomerular neuropil. (*E*,*F*). Protoplasmic astrocytes distributed in small groups. (*G*) Protoplasmic astrocytes oriented along the layer boundaries. (*H*) Radial-like cells. (*I*) Twin astrocytes. (*J*) Individual protoplasmic astrocytes surrounding the limits of the SEZ/RMS. (*K*) Poorly elaborated cells in small groups. (*L*,*M*) Radial-like cells sending their projections into the SEZ/RMS core and forming gliotunnels. This diagram was elaborated from the cell outlines.

Although the morphology of these cells was reminiscent of radial glia, their processes were shorter. Moreover, these processes frequently had numerous ramifications, conferring on them the aspect of an intermediate state between radial glia and a mature astrocyte (Fig. 8*B*). Usually, these cells were closely accompanied by sibling cells that shared the same signature (Fig. 8*A*,*B*).

Besides adult radial glia-like cells, we also found evidence of other forms of glia that were not fully developed, or reflected their proliferative potential. Particularly, we observed groups of cells akin to the astrocytic "isogenic groups" described by Cajal (Cajal 1913) in different species and structures (Fig. 8*D*–*F*). Owing to their centrosome position, Cajal concluded these cells were groups of related cells emerging from a recent mitosis (Cajal 1913). In our analysis, these clusters were made up of 2 to 6 cells, each with an astrocytic morphology and the same fluorescent signature (Fig. 8*E*,*F*). These cells asymmetrically projected their processes and arborizations in a centrifugal direction, frequently with their somata remaining in close apposition (Fig. 8*E*; Fig. 6*I*).

Astrocytes in the RMS: Morphology and Clonal Distribution

Due to the lack of methods to achieve appropriate targeting, little is known about astrocyte morphology and their clonal composition in the RMS. For this reason, we analyzed this region (horizontal arm, excluding the OB region) in adult sections of mice electroporated with Star Track at E14 (Fig. 9*A*–*L*; $n = 5$). Consistent with their prominent radial migration, labeled cells were exclusively located on the electroporated side of the RMS. The

Table 1 Quantitative analysis of astrocyte clones in the adult OB

Clone	Brain	Combination	# Cells	Slice: #Cells	Layers	Reference (Supplementary Figs 1–4)
1	1	001001101100	7	16:4/17:3	GR	291A–D; 374A–C
2	1	000001101111	8	13:2/14:6	GR	156A–B; 199A–F
3	1	000010101011	15	6:4/7:5/10:6	ONL/GL/EPL	15A–C; 16A–B; 8A–D; 58A–F;
4	1	000011101100	3	19:3	GR	450A–C
5	1	000101111111	9	5:2/15:5/16:2	GR	216A–C; 272A–B; 221A; 222A; 5A–B
6	1	000110110000	11	16:4/18:6/19:1	GR	432A–B; 460A; 292A–B; 275G; 260A; 435A–C; 433A
7	1	000110111111	1	9:1	ONL	41A
8	1	001000100011	2	9:1/10:1	EPL/GL	59A; 43A
9	1	001000110101	1	19:1	GR	457A
10	1	001011001111	2	10:2	ONL/GL	60A; 61A
11	1	001100001111	2	15:1/16:1	GR	240A; 259A
12	1	001100111100	65	7:1/8:12/9:23/10:19/11:9/12:1	GL/EPL/MT	21A–BJ; 10A; 84A
13	1	111110111111	5	13:2/14:3	MT	118A–B; 174A; 165A–B
14	1	111001110110	2	16:2	GR	278A–B
15	1	111001100110	6	12:1/13:1/14:3/15:1	GR	171A–C; 221A; 146A; 114A
16	1	110110101001	3	17:3	GR	345A–C
17	1	100000101110	7	16:3/17:3/19:1	GR	370A–C; 474A; 283A–C
18	1	101000111111	4	10:2/14:1/15:1	GR/MT	167A; 218A; 52A–B
19	1	101111101111	21	9:1/10:4/11:6/12:7/13:3	GL/IPL/EPL/GR/ONL	137A–B; 138A; 38A; 57A–D; 71A–F; 100A–G
20	1	101110111110	10	12:2/13:3/14:4/16:1	GL/ONL/GR	121A–C; 87A–B; 178A–D; 299A
21	1	001110000111	2	14:2	GR	180A–B
22	1	010000101100	7	12:4/16:3	EPL/GL	88A–D; 318A–C
23	1	010000101110	8	15:3/16:5	IPL/MT/EPL	211A–C; 304A–E
24	2	001001111111	6	22:3/23:3	GR/IPL	119A–F
25	2	101000111101	1	19:1	GR	74A
26	2	101101111110	1	12:1	GL	23A
27	2	111110000000	5	17:5	GR	64A–E
28	2	000001111111	12	10:7/11:1/12:2/15:1/16:1	GR/EPL/GL/ONL	12A–J; 44A; 57A
29	2	100000111110	13	14:1/15:2/16:8/17:2	EPL/GL	38A–M
30	2	101111111111	2	20: 2	GR	87A–B
31	3A	000011100101	1	7:1	GR	7A
32	3A	000100101111	1	9:1	GR	25A
33	3A	100001111111	1	9:1	GR	23A
34	3A	111111101111	4	8:1/10:3	GR, MT, GL	17A; 29A–B; 30A
35	3B	000001101100	1	19:1	GL	138A
36	3B	000100110110	7	27:1/28:6	GL/EPL/GR	323A; 333A–F
37	3B	000101101110	4	10:2/11:1/12:1	GR	18A; 28A; 13A–B
38	3B	000110101100	1	17:1	GR	87A
39	3B	001001101111	1	18:1	GL	105A
40	3B	001110111110	23	4:1/5:1/6:2/7:2/9:4/11:4/20:2/24:2/25:3/26:2	SEZ/GR/GL/ONL	1A–N; 185A–B; 280A–B; 296A–C; 311A–B
41	3B	001111111110	4	19:4	GR	159A–D
42	3B	111100100000	3	18:3	GR	124A–C

morphology of astrocytes varied largely depending on their location: radial cells and astrocytes with only a few poorly branched processes coincided within the migratory stream (Fig. 9*B*,*F*,*J*; Fig. 6*K*–*M*), whereas protoplasmic astrocytes were found around this region (Fig. 9*D*,*H*,*K*; Fig. 6*J*). At the clonal level, we found small groups of astrocytes sharing the same fluorescent signature in close proximity, suggesting that they arose from a recent cell division (Fig. 9*C*). Because GFAP$^+$ progenitors continue to produce neuroblasts in the adult RMS (Alonso et al. 2008), these cells could retain a fluorescent signature for some days after GFAP promoter inactivation. To ensure that these neuroblasts were not included in our analysis, we performed immunohistochemistry for GFAP (Fig. 9*A*–*L*). We found very few cells lacking GFAP and most of these cells had a clearly distinct morphology to astrocytes, exhibiting a small soma with only one or 2 smooth processes typical from neuroblasts (Fig. 9*G*,*J* arrowheads). The rest of the labeled cells expressed different levels of GFAP, including those with a poorly elaborated morphology (Fig. 9*C*).

As the olfactory ventricle at this level also produces astroglia that disperse into the adjacent regions, we expected to find clones occupying both the RMS and the parenchyma (Fig. 9*M*–*R*). However, this distribution was very infrequent and most of the parenchymal clones did not leave any trace in the RMS (Fig. 9*O*–*R*, arrows).

Discussion

Technical limitations have previously hindered studies aimed at describing how astrocyte clones are organized in the OB, including the inability of retroviruses to target OB glia (Reid et al. 1999). The Star Track technique overcomes this problem and has allowed us to elaborate a map of the astrocyte families in the OB and RMS. In general, these populations were characterized by

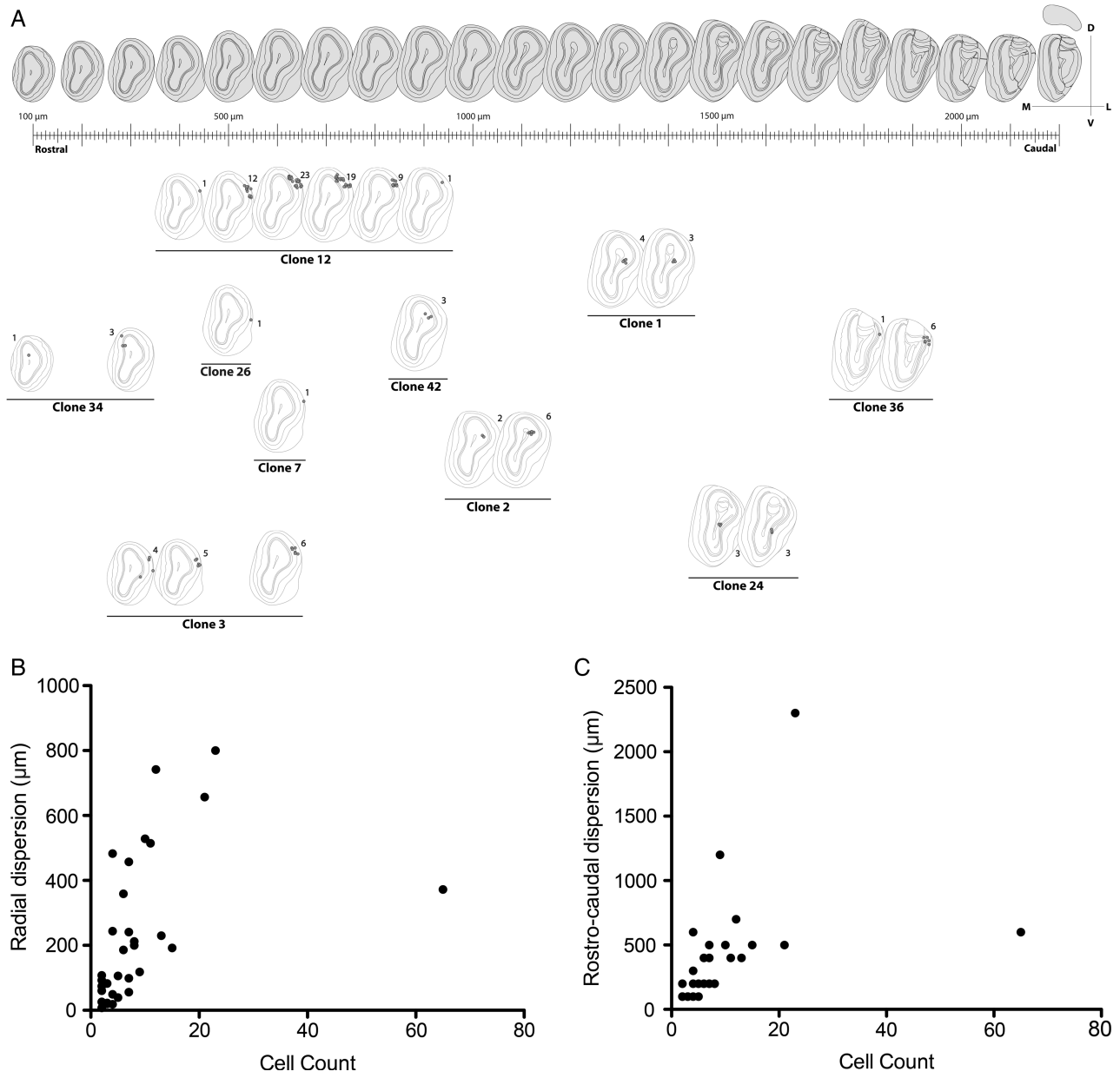

Figure 7. Quantitative analysis of clonal distribution. (*A*) Diagram depicting the clonal distribution that was elaborated by projecting part of our data (Table 1) over a reference atlas (Lein et al. 2007). (*B*,*C*) Correlation analysis between clonal cell count and radial (B; Spearman correlation, $P < 0.0001$; $\rho = 0.72$) or rostrocaudal dispersion (C; Spearman correlation, $P < 0.0001$; $\rho = 0.77$).

their morphological diversity, clonal features and by the existence of immature astrocytes.

Targeting Glial Populations nonaccessible to Previous Clonal Analyses

Clonal analysis based on retroviral labeling has made it possible to elaborate a clonal map of neurons and glia in most brain regions (Price and Thurlow 1988; Walsh and Cepko 1988, 1992; Luskin et al. 1993; McCarthy et al. 2001). However, this approach has proved unsuitable to target certain glial subtypes, such as NG2-cells, *glia limitans* or the entire OB glia population (Reid et al. 1999; McCarthy et al. 2001). Since intraventricular retroviral injections only target mitotic cells in contact with cerebrospinal fluid, numerous glial progenitors escape retroviral labeling, at least at certain developmental stages. Indeed, retroviral injection in neonates did label a small proportion of the NG2 and OB glia populations (Levison et al. 1999; Suzuki and Goldman 2003). A further inconvenience is that retroviruses are prone to epigenetic silencing, which could also affect reporter expression in specific cell types (Pannell and Ellis 2001). These problems do not seem to affect the efficiency of Star Track, allowing a clonal analysis of these populations to be performed.

Gliogenesis in the OB/RMS: Origin, Dispersion, and Morphology

In the cerebral cortex, astrocytes arise from radial glia, either directly or through an intermediate progenitor. In both cases their migratory pathway is similar, emerging from proliferative layers

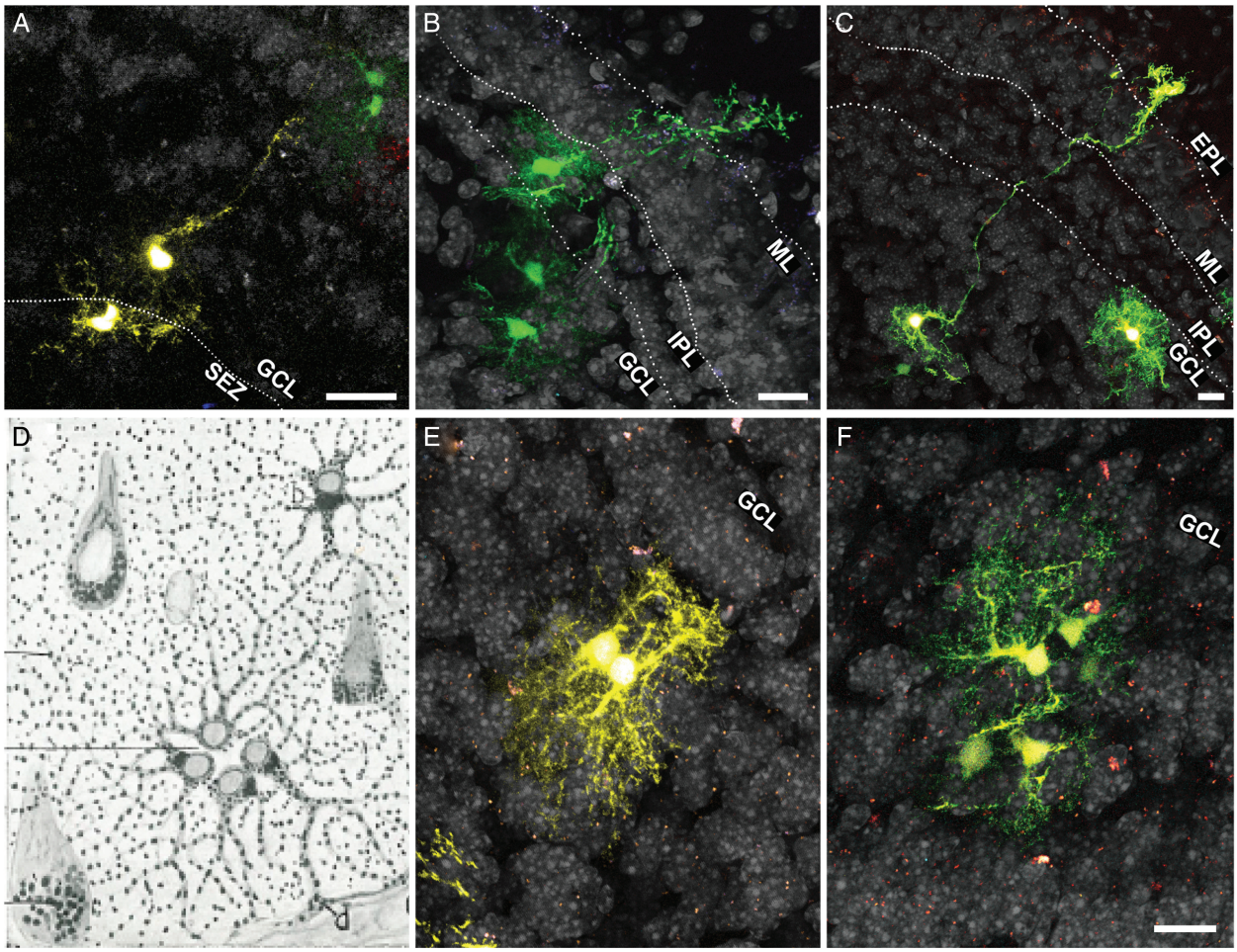

Figure 8. Immature glia in the adult OB. (*A–C*) Astroglia exhibiting an intermediate morphology between radial glia and a protoplasmic astrocyte. Note the presence of sibling cells with the same fluorescent signature accompanying these potential immature cells. (*D*) A drawing by Cajal showing an isogenic group composed of 4 astrocytes (quadriga) in the gray matter of the human brain. (*E,F*) Isogenic groups of 2 (*E*; twin astrocytes) or 5 cells (*F*). In these groups the cells orientate their processes in the opposite direction to the cleavage plane. Scale bars = 25 μm in *A–C*, *E,F* (shown in *F*).

(SVZ/VZ) and following the course of the radial glial processes (Suzuki and Goldman 2003). In contrast, the origin and the migratory pathways used by OB and RMS astrocytes have remained elusive. Here, we demonstrate that this population is generated from local progenitors and that the cortical VZ/SVZ do not contribute to these populations, which confirms previous evidence in post-natal animals (Suzuki and Goldman 2003). This conclusion is further supported by the lack of glial labeling in the nonelectroporated side. If OB/RMS glia were to arise in posterior regions, the lack of labeling in the nonelectroporated side could be explained by 2 very unlikely hypotheses: (1) asymmetric migration of glial progenitors exclusively along one side of the RMS; or (2) the subsequent rearrangement on one of sides of the RMS after a more disorganized migration. However, as the precision of our electroporation was limited, we cannot rule out very short-range tangential migrations from the lateral ventricle SVZ to the proximal RMS or from the rostral RMS to the OB. In fact, direct radial glia transformation could also contribute tangentially, as their processes run in parallel to portions of the RMS (Alves et al. 2002). Moreover, it has been suggested that the adult cortical SVZ generates glia destined to enter the RMS (Sohn et al. 2015). What is now clearer is that the glia from the RMS ventricle contributes to adjacent areas, such as anterior olfactory nucleus, tenia tecta or the piriform nucleus. However, as occurs with the OB, most of clones in the parenchyma did not leave any trace in the RMS.

Our analysis also revealed the radial arrangement of the OB/RMS glia, as reflected by the fan-like dispersion rooted in the olfactory ventricle. There are 3 potential hypotheses that could explain this pattern: (1) progenitors giving rise to post-mitotic glia that migrate to their final position; (2) glial progenitors migrate to their final position then start to proliferate; or (3) glial progenitors migrate and proliferate at the same time. The first hypothesis would involve an ordered migration of sibling post-mitotic cells to the same OB area, which is very unlikely in the light of previous findings in cortex (García-Marqués and López-Mascaraque 2012; Ge et al. 2012). Conversely, the second scenario would produce perfect spherical clusters, which would contradict our dispersion analysis that rules out a purely passive volumetric expansion resulting from cell division and rather, it highlights an increased variance with cell count. This can only be explained if short-range migrations also take place, which makes the third scenario the most plausible. Interestingly, only one of the clones contributed cells to the SEZ, which suggest that those progenitors in the proliferative regions also ultimately migrate to other layers. Based on these conclusions, we propose 3

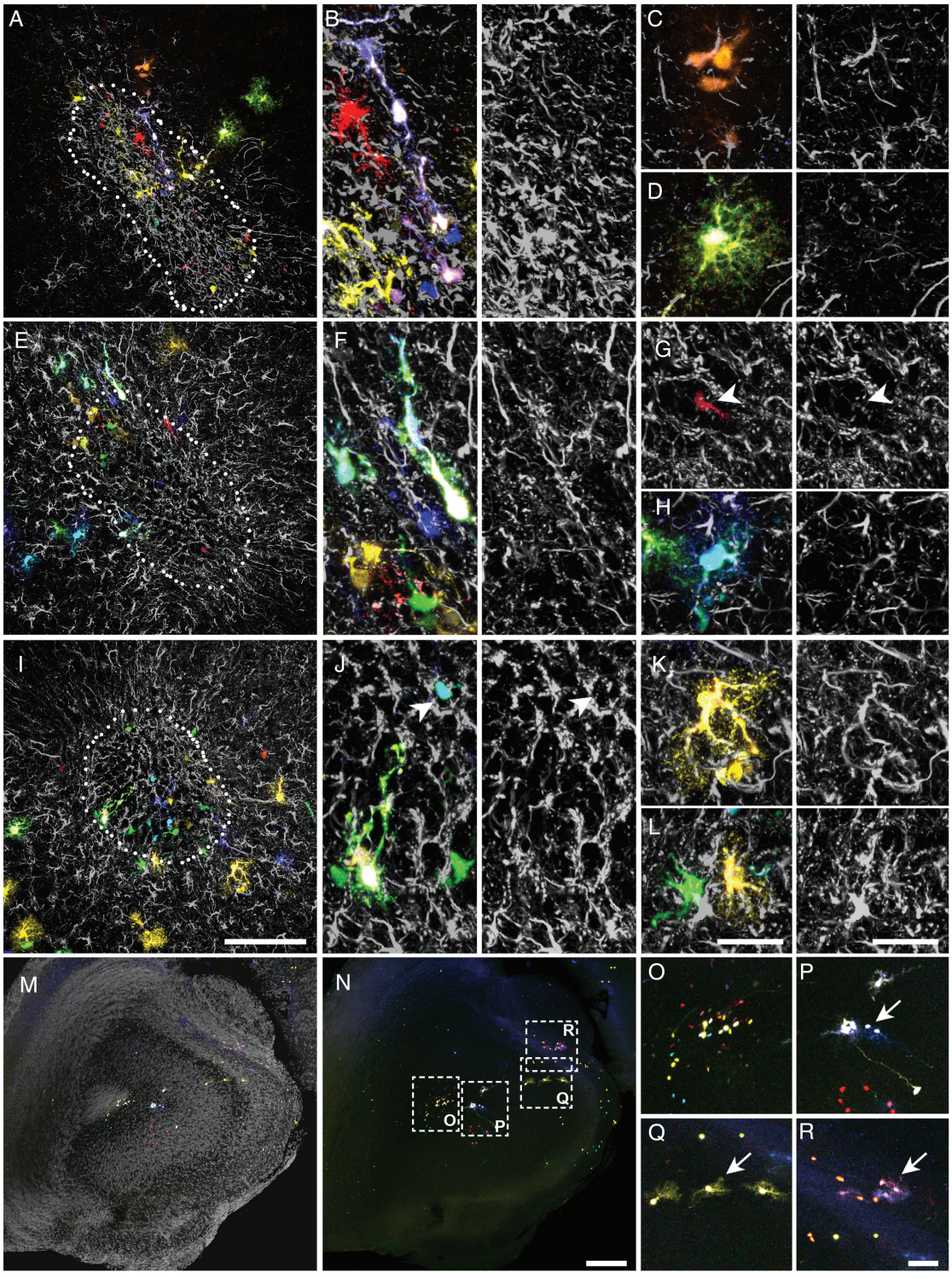

Figure 9. Astroglial clones in the RMS. (*A–L*). Different views of the RMS in coronal sections. (*A,E,I*) Low magnifications. (*B,F,J*) High magnifications showing radial-like astroglia. (*C*) High magnification of an isogenic group comprised of 3 sibling cells with the same fluorescent signature. (*D,H,K,L*) Protoplasmic-like astrocytes in the RMS margins. (*G*) Neuroblast within a migratory chain. Note its smaller soma size and the lack of GFAP expression. (*M,N*) Low magnification of RMS and adjacent areas (anterior olfactory nucleus) with (*M*) or without nuclear counterstaining in gray (*N*). (*O*) High magnification of inset in *N* showing the RMS labeling. (*P–R*) High magnification of insets in *N* showing examples of clones with no representation in the RMS. Scale bars = 100 μm in *A,E,I* (shown in *I*); 25 μm in *B–D*, *F–H*, *J–L* (shown in *L*); 200 μm in *M*, *N* (shown in *N*); 50 μm in *O–R* (shown in *R*).

phases of OB/RMS astrogliogenesis: (1) intermediate progenitors arise in the local VZ/SVZ; (2) radial migration with some rostro/caudal contribution; (3) proliferation and short-range tangential/radial movements. This picture would be completed with some single-cell clones derived from radial glia transformation. Such a scheme is very similar to the events observed in

the cerebral cortex (Suzuki and Goldman, 2003; Ge et al. 2012; García-Marqués and López-Mascaraque 2012) and it may possibly be applicable to the rest of the CNS.

Despite their similar pattern of generation, astrocytes in the OB exhibited tremendous morphological variation compared with cortical astrocytes. It remains to be determined whether such extraordinary variety is the morphological response to the anatomy of this structure or it hides a functional specialization. Astrocytes exhibit remarkable morphological plasticity, particularly in response to brain injury (reviewed in Ridet et al. 1997; Martín-López et al. 2013). This involves hypertrophy of astrocytic processes and the formation of lamellar structures to surround the damaged parenchyma. This resembles the morphology in the ONL, where astrocytes are arranged as sheets in a similar way to the pial astrocytes in the cerebral cortex (Holen 2011; García-Marqués and López-Mascaraque 2012), or they project thick processes towards the GL. This sheet-like arrangement seems to facilitate their function as barriers, maximizing the cytoplasmic extensions that are in contact with the lesion or brain surface.

The GL is populated by astrocytes with large processes and exuberant branching. Such a morphology coincides with the wedge-shape (Bailey and Shipley 1993; Chiu and Greer 1996) or velate astrocytes described in this region (Valverde and López-Mascaraque 1991). Astrocytes co-habit these layers with ensheathing cells that originate in the olfactory placode (Doucette 1989; Blanchart et al. 2011), which serve as a functional relay of astrocytes beyond the brain. Interestingly, both these glial types share a similar function and a similar morphology, despite their different origins. In the ML, oGCL, and plexiform layers, astrocytes mainly adopt a typical protoplasmic morphology, corresponding to the circular and semicircular astrocytes described previously (Bailey and Shipley 1993; Chiu and Greer 1996). This morphology seems to reflect their function in neuronal support and synaptic modulation (Halassa et al. 2007). Moreover, we found less elaborate morphologies in the SEZ and dGCL, as well as radial-like cells and isogenic groups scattered throughout different layers (Cajal 1913; Emsley et al. 2012; Larriva-Sahd 2014). The similarity between these cells and immature glia suggests that rather than serving a specific function, these morphologies reflect either a failure to differentiate or the presence of active progenitors generating immature cells. This latter hypothesis is strongly supported by other studies in which radial glia-like cells are seen to be generated in the adult OB (Emsley et al. 2012). Interestingly, such intermediate cells, with morphological features between a radial glia and an astrocyte, have also been described as type-B progenitors involved in adult neurogenesis (Liu et al. 2006).

Distribution and Features of Astrocyte Clones in the OB/RMS

Based on their centrosome location, "opposed to the plane of contact", Cajal described "isogenic groups" of cells (Cajal 1913), suggesting these were comprised of sibling cells generated by a recent mitosis. As mentioned above, until recently there has been no appropriate method to study the OB and RMS, and thus, here we present the first map of the families of astrocytes that develop in these regions. Astrocyte clones differed in their cell number and while some were composed of up to 65 cells, ~24% of them were single cells. Such variability could be sustained by different developmental mechanisms governing the well-known origins of astrocytes (reviewed in Levison and Goldman 1993): multiple-cell clones would be derived from intermediate progenitors and single-cell clones might represent astrocytes transformed from radial glia that would not contribute to other astroglia clones. Programmed cell death could also be decisive to regulate the ultimate size of the clusters (reviewed in Yamaguchi and Miura 2015). Likewise, the distinct temporal origins must also be considered, whereby larger clones might emerge earlier when no other clone would compete with it for space. Interestingly, the average clonal size was considerably smaller than that of cortical astrocytes (Luskin et al. 1988; García-Marqués and López-Mascaraque 2012) and it could be argued that a larger parenchymal extension in the cortex permits more proliferation. However, additional reasons might underlie this difference, particularly since other glial populations, like NG2-glia clones, were comprised of a comparable number of cells in both regions (García-Marqués et al. 2014).

In the rostrocaudal axis, clones formed cellular clusters that occupy contiguous sections. Indeed, only 2 clones (#5 and #40) were found in 2 remote locations along the rostrocaudal axis (≈1 mm apart), which might represent a rare migratory event or the unlikely occurrence of the same signature appearing twice in independent electroporation events. Furthermore, as in other brain regions (Luskin et al. 1988; García-Marqués and López-Mascaraque 2012), astrocyte clones did not respect the OB layer organization but rather, their extension depended on their cell number. In this respect, the only clear organization occurred around the olfactory glomeruli. Here, astrocyte clones were mostly concentrated in a single or few adjacent glomeruli, confirming that not only single astrocytes (Bailey and Shipley 1993) but also astrocyte clones are relatively loyal to a single glomerulus. While the somata of most of the cells occupy interglomerular walls, in some clones cells did gain access to the glomerular neuropil. This is in contrast with the barrel cortex, where we failed to find any particular clonal organization of astrocytes despite the relatively similar anatomical organization. Such clonal organization could be a plastic response to the peculiar anatomy of this region or it may emerge as the structural correlate of some underlying function. In analogy to the preferential electrical communication among sibling neurons occurring during development (Yu et al. 2012), such clonal compartmentalization could modulate sensorial information coming from the olfactory epithelium. A preferential communication via gap junctions between astrocytes within glomeruli compared with astrocytes from adjacent glomeruli seems to support that hypothesis (Roux et al. 2011). In addition, this clonal organization might also play a role in the aggregation of olfactory axons and the mitral cell dendrite into a single glomerulus during development (Bailey and Shipley 1993).

The OB/RMS Generates a Singular Astrocyte Population: Functional Implications

Distinct CNS regions differ greatly in their astroglial composition, to the extent that discrete regions can be defined solely on the morphology, density, and proliferation rate of their astroglia (Emsley and Macklis 2006). Based on our results, OB/RMS astrocytes share few similarities and they display many differences from other well-described CNS areas like the cerebral cortex. In both, the OB and cerebral cortex, we found a remarkable presence of pial clones, with most of their cells forming sheets parallel to the brain surface. Moreover, astroglia in these areas are generated in a very similar pattern. In contrast, OB and/or RMS astroglia differ in many aspects from those in the cerebral cortex, including: (1) smaller clonal size; (2) greater morphological heterogeneity within each clone; (3) a lack of large columnar clones associated

to single blood vessels (see Fig. 5G–J in García-Marqués and López-Mascaraque 2012); (4) the presence of radial-like cells and isogenic groups. These differences might be a consequence of the gliogenesis that takes place over 2 different timescales in the OB/RMS and cortex. However, this could not explain why we did find similar patterns when electroporations were performed at E13 or E15 (data not shown), consistent with the fact that the bulk of gliogenesis occurs after E16 (Bayer and Altman 1991; Sauvageot and Stiles 2002).

There may be functional consequences associated with the particular characteristics of these astroglial populations. In different vertebrates, including infant humans (Sanai et al. 2011), the OB and RMS are part of the migratory pathway used by neuroblasts that move from the SVZ to the OB during adult neurogenesis (Altman 1969). A large astroglial population supports this migration during both phases (Peretto et al. 1997; Mason et al. 2001; Bolteus and Bordey 2004). We previously demonstrated that neuroblasts from a RMS explant migrate further and faster over astrocyte monolayers derived from the OB and RMS, than over those from the cerebral cortex or other areas adjacent to the RMS (García-Marqués et al. 2010). We then hypothesized that similarities between OB and RMS astrocytes could define a permissive pathway, in contrast to other nonpermissive adjacent regions. This hypothesis is in line with the dissimilarities we found between the OB/RMS and cortical astroglia, particularly regarding the presence of immature forms. An immature microenvironment might be analogous to embryonic tissue, where most neuronal migration occurs. Alternatively, the singularity in the OB/RMS astroglial population could also arise as a consequence of having to support such substantial migration. On the basis of this hypothesis, neuroblasts may release molecular factors that promote astrocyte immaturity, as they do to clear the path of astrocytic processes (Kaneko et al. 2010). This would explain why other regions adjacent to the RMS, whose astrocytes also emerge from the olfactory ventricle, are not permissive to this migration. Future in vivo experiments should clarify whether these singularities have a functional correlate or if they entail irrelevant biological variance.

Supplementary Material

Supplementary material can be found at: http://www.cercor.oxfordjournals.org/online.

Funding

This work was supported by the Spanish Ministry of Economy and Competitiveness (grant number BFU2013-48807-R).

Notes

We thank Raul Núñez-Llaves and Sandra Rodriguez for her excellent technical support and Mark Sefton for helpful editorial assistance. *Conflict of Interest*: None declared.

References

Alonso M, Ortega-Pérez I, Grubb MS, Bourgeois JP, Charneau P, Lledo PM. 2008. Turning astrocytes from the rostral migratory stream into neurons: a role for the olfactory sensory organ. J Neurosci. 28:11089–11102.

Altman J. 1969. Autoradiographic and histological studies of postnatal neurogenesis. IV. Cell proliferation and migration in the anterior forebrain, with special reference to persisting neurogenesis in the olfactory bulb. J Comp Neurol. 137:433–458.

Alves JA, Barone P, Engelender S, Fróes MM, Menezes JR. 2002. Initial stages of radial glia astrocytic transformation in the early postnatal anterior subventricular zone. J Neurobiol. 52:251–265.

Bailey MS, Shipley MT. 1993. Astrocyte subtypes in the rat olfactory bulb: morphological heterogeneity and differential laminar distribution. J Comp Neurol. 328:501–526.

Bayer SA, Altman J. 1991. Neocortical development. New York (NY): Raven Press.

Blanchart A, Martín-López E, De Carlos JA, López-Mascaraque L. 2011. Peripheral contributions to olfactory bulb cell populations (migrations towards the olfactory bulb). Glia. 59:278–292.

Bolteus AJ, Bordey A. 2004. GABA release and uptake regulate neuronal precursor migration in the postnatal subventricular zone. J Neurosci. 24:7623–7631.

Cajal SR. 1913. Contribución al conocimiento de la neuroglia del cerebro humano. Trab Lab Invest Biol. 11:255–315.

Chaboub LS, Deneen B. 2012. Developmental origins of astrocyte heterogeneity: the final frontier of CNS development. Dev Neurosci. 34:379–388.

Chiu K, Greer CA. 1996. Immunocytochemical analyses of astrocyte development in the olfactory bulb. Dev Brain Res. 95:28–37.

Doucette R. 1989. Development of the nerve fiber layer in the olfactory bulb of mouse embryos. J Comp Neurol. 285: 514–527.

Emsley JG, Macklis JD. 2006. Astroglial heterogeneity closely reflects the neuronal-defined anatomy of the adult murine CNS. Neuron Glia Biol. 2:175–186.

Emsley JG, Menezes JR, Madeiro Da Costa RF, Martinez AM, Macklis JD. 2012. Identification of radial glia-like cells in the adult mouse olfactory bulb. Exp Neurol. 236:283–297.

García-Marqués J, De Carlos JA, Greer CA, López-Mascaraque L. 2010. Different astroglia permissivity controls the migration of olfactory bulb interneuron precursors. Glia. 58:218–230.

García-Marqués J, López-Mascaraque L. 2012. Clonal identity determines astrocyte cortical heterogeneity. Cereb Cortex. 23:1463–1472.

García-Marqués J, Núñez-Llaves R, López-Mascaraque L. 2014. NG2-glia from pallial progenitors produce the largest clonal clusters of the brain: time frame of clonal generation in cortex and olfactory bulb. J Neurosci. 34:2305–2313.

Ge WP, Miyawaki A, Gage FH, Jan YN, Jan LY. 2012. Local generation of glia is a major astrocyte source in postnatal cortex. Nature. 484:376–380.

Halassa MM, Fellin T, Takano H, Dong JH, Haydon PG. 2007. Synaptic islands defined by the territory of a single astrocyte. J Neurosci. 27:6473–6477.

Hochstim C, Deneen B, Lukaszewicz A, Zhou Q, Anderson DJ. 2008. Identification of positionally distinct astrocyte subtypes whose identities are specified by a homeodomain code. Cell. 133:510–522.

Holen T. 2011. The ultrastructure of lamellar stack astrocytes. Glia. 59:1075–1083.

Kaneko N, Marín O, Koike M, Hirota Y, Uchiyama Y, Wu JY, Lu Q, Tessier-Lavigne M, Alvarez-Buylla A, Okano H, et al. 2010. New neurons clear the path of astrocytic processes for their rapid migration in the adult brain. Neuron. 67:213–223.

Larriva-Sahd. 2014. Structural variation and interactions among astrocytes of the rostral migratory stream and olfactory bulb: II. Golgi and electron microscopy study of the rat. Neurosci Res. 89:10–30.

Lein ES, Hawrylycz MJ, Ao N, Ayres M, Bensinger A, Bernard A, Boe AF, Boguski MS, Brockway KS, Byrnes EJ, et al. 2007. Genome-wide atlas of gene expression in the adult mouse brain. Nature. 445:168–176.

Levison SW, Goldman JE. 1993. Both oligodendrocytes and astrocytes develop from progenitors in the subventricular zone of postnatal rat forebrain. Neuron. 10:201–212.

Levison SW, Young GM, Goldman JE. 1999. Cycling cells in the adult rat neocortex preferentially generate oligodendroglia. J Neurosci Res. 57:435–446.

Liu X, Bolteus AJ, Balkin DM, Henschel O, Bordey A. 2006. GFAP-expressing cells in the postnatal subventricular zone display a unique glial phenotype intermediate between radial glia and astrocytes. Glia. 54:394–410.

Luskin MB, Parnavelas JG, Barfield JA. 1993. Neurons, astrocytes, and oligodendrocytes of the rat cerebral cortex originate from separate progenitor cells: an ultrastructural analysis of clonally related cells. J Neurosci. 13:1730–1750.

Luskin MB, Pearlman AL, Sanes JR. 1988. Cell lineage in the cerebral cortex of the mouse studied in vivo and in vitro with a recombinant retrovirus. Neuron. 1:635–647.

Martín-López E, García-Marqués J, Núñez-Llaves R, López-Mascaraque L. 2013. Clonal astrocytic response to cortical injury. PloS One. 8:e74039.

Mason HA, Ito S, Corfas G. 2001. Extracellular signals that regulate the tangential migration of olfactory bulb neuronal precursors: Inducers, inhibitors, and repellents. J Neurosci. 21:7654–7663.

Matyash V, Kettenmann H. 2009. Heterogeneity in astrocyte morphology and physiology. Brain Res Rev. 63:2–10.

McCarthy M, Turnbull DH, Walsh CA, Fishell G. 2001. Telencephalic neural progenitors appear to be restricted to regional and glial fates before the onset of neurogenesis. J Neurosci. 21:6772–6781.

Oberheim NA, Goldman SA, Nedergaard M. 2012. Heterogeneity of astrocytic form and function. Methods Mol Biol. 814: 23–45.

Pannell D, Ellis J. 2001. Silencing of gene expression: implications for design of retrovirus vectors. Rev Med Virol. 11:205–217.

Peretto P, Merighi A, Fasolo A, Bonfanti L. 1997. Glial tubes in the rostral migratory stream of the adult rat. Brain Res Bull. 42:9–21.

Price J, Thurlow L. 1988. Cell lineage in the rat cerebral cortex: a study using retroviral-mediated gene transfer. Development. 104:473–482.

Reid CB, Liang I, Walsh CA. 1999. Clonal mixing, clonal restriction, and specification of cell types in the developing rat olfactory bulb. J Comp Neurol. 403:106–118.

Ridet JL, Malhotra SK, Privat A, Gage FH. 1997. Reactive astrocytes: cellular and molecular cues to biological function. Trends Neurosci. 20:570–577.

Roux L, Benchenane K, Rothstein JD, Bonvento G, Giaume C. 2011. Plasticity of astroglial networks in olfactory glomeruli. Proc Natl Acad Sci USA. 108:18442–18446.

Sanai N, Nguyen T, Ihrie RA, Mirzadeh Z, Tsai HH, Wong M, Gupta N, Berger MS, Huang E, Garcia-Verdugo JM, et al. 2011. Corridors of migrating neurons in the human brain and their decline during infancy. Nature. 478:382–386.

Sauvageot CM, Stiles CD. 2002. Molecular mechanisms controlling cortical gliogenesis. Curr Opin Neurobiol. 12: 244–249.

Schindelin J, Arganda-Carreras I, Frise E, Kaynig V, Longair M, Pietzsch T, Preibisch S, Rueden C, Saalfeld S, Schmid B, et al. 2012. Fiji: an open-source platform for biological-image analysis. Nat Methods. 9:676–682.

Sohn J, Orosco L, Guo F, Chung SH, Bannerman P, Mills Ko E, Zarbalis K, Deng W, Pleasure D. 2015. The subventricular zone continues to generate corpus callosum and rostral migratory stream astroglia in normal adult mice. J Neurosci. 35:3756–3763.

Suzuki SO, Goldman JE. 2003. Multiple cell populations in the early postnatal subventricular zone take distinct migratory pathways: a dynamic study of glial and neuronal progenitor migration. J Neurosci. 23:4240–4250.

Valverde F, López-Mascaraque L. 1991. Neuroglial arrangements in the olfactory glomeruli of the hedgehog. J Comp Neurol. 307:658–674.

Walsh C, Cepko CL. 1988. Clonally related cortical cells show several migration patterns. Science. 241:1342–1345.

Wang D, Bordey A. 2008. The astrocyte odyssey. Prog Neurobiol. 86:342–367.

Yamaguchi Y, Miura M. 2015. Programmed cell death in neurodevelopment. Dev Cell. 32:478–490.

Yu YC, He S, Chen S, Fu Y, Brown KN, Yao XH, Ma J, Gao KP, Sosinsky GE, Huang K, et al. 2012. Preferential electrical coupling regulates neocortical lineage-dependent microcircuit assembly. Nature. 486:113–117.

Zhang Y, Barres BA. 2010. Astrocyte heterogeneity: an underappreciated topic in neurobiology. Curr Opin Neurobiol. 20: 588–594.